Ectodermal Wnt signalling, cell fate determination and polarity of the skate gill arch skeleton

Jenaid M. Rees[1], Victoria A. Sleight[2], Stephen J. Clark[3], Tetsuya Nakamura[4] and J. Andrew Gillis[1,5,*]

[1]Department of Zoology, University of Cambridge, U.K.
[2]School of Biological Sciences, University of Aberdeen, U.K.
[3]Babraham Institute, U.K.
[4]Department of Genetics, Rutgers University, U.S.A.
[5]Josephine Bay Paul Center for Comparative Molecular Biology and Evolution, Marine Biological Laboratory, U.S.A.

*Correspondence: agillis@mbl.edu

The gill skeleton of cartilaginous fishes (sharks, skates, rays and holocephalans) exhibits a striking anterior–posterior polarity, with a series of fine appendages called branchial rays projecting from the posterior margin of the gill arch cartilages. We previously demonstrated in the skate (*Leucoraja erinacea*) that branchial rays derive from a posterior domain of pharyngeal arch mesenchyme that is responsive to Shh signalling from a distal gill arch epithelial ridge (GAER) signalling centre. However, how branchial ray progenitors are specified exclusively within posterior gill arch mesenchyme is not known. Here we show that genes encoding several Wnt ligands are expressed in the ectoderm immediately adjacent to the skate GAER, and that these Wnt signals are transduced largely in the anterior arch environment. Using pharmacological manipulation, we show that inhibition of Wnt signalling results in an anterior expansion of Shh signal transduction in developing skate gill arches, and in the formation of ectopic anterior branchial ray cartilages. Our findings demonstrate that ectodermal Wnt signalling contributes to gill arch skeletal polarity in skate by restricting Shh signal transduction and chondrogenesis to the posterior arch environment and highlights the importance of signalling interactions at embryonic tissue boundaries for cell fate determination in vertebrate pharyngeal arches.

Introduction

The pharyngeal arches of vertebrates are a series of paired columns of tissue that form on either side of the embryonic head. Pharyngeal arches form as iterative outpockets of foregut endoderm contact the overlying surface ectoderm, and this meeting of endoderm and ectoderm generates columns lined laterally by ectoderm, medially by endoderm, and containing a core of mesoderm and neural crest-derived mesenchyme (Graham and Smith, 2001). In fishes, endodermal outpockets fuse with the overlying surface ectoderm, giving rise to the gill slits and the respiratory surfaces of the gills (Gillis and Tidswell, 2017). In amniotes, endodermal outpockets give rise to glandular tissues, such as the tonsils, parathyroid and ultimobranchial glands (Grevellec and Tucker, 2010). The largely neural crest-derived mesenchyme of the pharyngeal arches gives rise to the pharyngeal skeleton – i.e., the skeleton of the jaws and gills in fishes, and of the jaw, auditory ossicles, and larynx in amniotes (Jiang et al., 2002, Kague et al., 2012, Sleight and Gillis, 2020, Couly and Le Douarin, 1990) – with mesenchymal derivatives of each arch receiving patterning and polarity information via signals from adjacent epithelia (Veitch et al., 1999, Gillis et al., 2009a, Couly et al., 2002, Brito et al., 2006). Pharyngeal arches are named according to their ancestral skeletal derivatives: the 1st pharyngeal arch is termed the mandibular arch, the 2nd pharyngeal arch is the hyoid arch, while the caudal pharyngeal arches are collectively termed the gill arches. In fishes, the gill arches give rise to a series of skeletal “arches” that support the lamellae of the gills.

All jawed vertebrates belong to one of two lineages: cartilaginous fishes (sharks, skates, rays and holocephalans) or bony vertebrates (ray- and lobe-fined fishes, with the latter including tetrapods). While the gill arch skeleton of both cartilaginous and bony fishes ancestrally consisted proximally of two principal gill arch cartilages (the epi- and ceratobranchials), the gill arch skeleton of cartilaginous fishes additionally includes a distal series of fine cartilaginous rods called branchial rays (Fig. 1A-C). These rays reflect the clear anteroposterior polarity of the gill arch skeleton of cartilaginous fishes, originating along the posterior margin of the epi- and ceratobranchial cartilages, and curving posteriorly as they project into the interbranchial septum of each arch (Gillis et al., 2009b). Elasmobranch cartilaginous

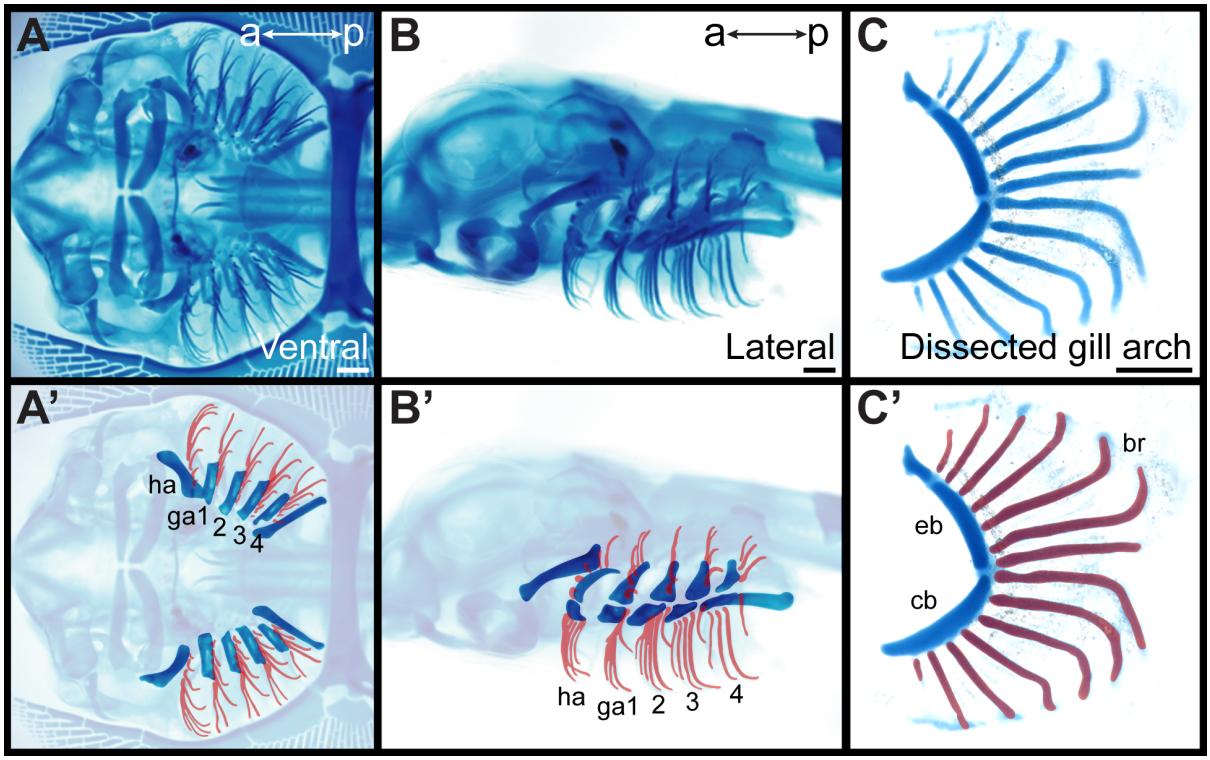

Figure 1: Overview of skate gill arch skeletal anatomy. Skeletal preparation of a S33 skate embryo in **(A)** ventral and **(B)** lateral view. In **(A')** and **(B')** the gill arches and branchial rays are highlighted, with branchial rays false-coloured red. Note that branchial rays project from the posterior margin of the hyoid and first four gill arches. **(C)** A dissected gill arch with the **(C')** dorsal epibranchial and ventral ceratobranchial gill arch cartilages indicated, and with branchial rays false-coloured red. a–p indicates anterior-posterior axis. br: branchial ray, cb: ceratobranchial, eb: epibranchial, ga1-4: gill arches 1-4, ha: hyoid arch, ma: mandibular arch. Scale bars: 1mm.

fishes (sharks, skates and rays) possess five sets of branchial rays, associated with their hyoid and first four gill arches. Holocephalans, on the other hand, possess a single set of branchial rays supporting their hyoid arch-derived operculum.

The branchial rays of cartilaginous fishes develop under the influence of the gill arch epithelial ridge (GAER): a *Sonic hedgehog* (*Shh*)-expressing signalling centre located within the posterior-distal epithelium of the gill arches (Gillis et al., 2009b; Gillis and Hall, 2016). As the gill arches undergo a prolonged phase of lateral expansion, Shh signalling from the GAER is asymmetrically transduced within the posterior arch environment, as evidenced by posterior expression of *Ptc2* – a Shh co-receptor and transcriptional readout of Shh signalling (Pearse et al., 2001). This posterior transduction of Shh signalling, in turn, appears to underlie the anteroposterior polarity of the gill arch skeleton: in skate, branchial rays derive exclusively from posterior–distal (Shh-responsive/GAER-adjacent) gill arch mesenchyme, application of exogenous Shh protein within gill arches is sufficient to induce ectopic branchial ray formation, and targeted or systemic inhibition of hedgehog signalling using cyclopamine results in branchial ray deletion (Gillis et al., 2009b; Gillis and Hall, 2016). However, whether other signalling mechanisms function alongside or in conjunction with GAER Shh signalling to establish and maintain gill arch skeletal polarity remains unexplored.

Here, we show in the little skate (*Leucoraja erinacea*) that the ectoderm immediately adjacent to the GAER expresses several genes encoding Wnt ligands. These Wnt signals are transduced in the anterior arch environment in a pattern that is broadly complementary to the posterior transduction of GAER Shh signalling. Inhibition of Wnt signalling in developing skate embryos results in an anterior expansion of Shh signalling transduction, and in the formation of ectopic branchial rays in the anterior gill arch. We propose that Wnt signalling from pharyngeal arch ectoderm contributes to maintenance of anterior–posterior polarity of the skate gill arch skeleton by repressing Shh signalling and chondrogenesis to the posterior gill arch territory.

Results

Wnt gene expression in the skate GAER and GAER-adjacent epithelium

In developing skate gill arches, Shh is expressed in the GAER (Fig. 2A), and branchial rays develop from a GAER-responsive domain of posterior arch mesenchyme (Gillis and Hall, 2016). To further explore the transcriptional environment of the GAER and to discover additional gene expression features that may contribute to gill arch polarity, we conducted a comparative transcriptomic and differential gene expression analysis of GAER and non-GAER regions of the first gill arch of the embryonic skate. Briefly, we manually dissected the **1)** GAER and **2)** non-GAER (control) regions from the first gill arch of stage (S)26 skate embryos (n=5; Fig. 2B–Bi), and we performed RNA extraction, library preparation, and RNAseq analysis on these samples. For the GAER region of the first gill arch, we included the whole distal tip of the arch in our dissection to ensure that the *Shh*-expressing GAER and adjacent Shh-responsive (i.e., *Ptc2*+) tissues were captured for this analysis (Fig. 2C-D). Following *de novo* transcriptome assembly, we tested for differential gene expression between GAER and non-GAER tissues (after first testing for differential expression of *Shh* in the GAER region, to confirm dissection accuracy). We used a false discovery rate of 5% and no log fold-change (LogFC) cut-off to generate a list of 401 genes that were upregulated in the GAER region. We sorted this list for genes encoding signalling pathway components and transcription factors with a log-fold change >2. (Fig. 2E). Differentially expressed genes were subjected to functional enrichment analysis, and this analysis indicated enrichment of Wnt signalling pathway components in GAER region (Fig. 2 Supplement 1 for enrichment analysis). Differentially expressed genes in the GAER region included those encoding the Wnt ligands Wnt2b, Wnt3, Wnt4, Wnt7b and Wnt9, the transmembrane Wnt inhibitors Kremen1 (Mao et al., 2002) and APCDD1 (Shimomura et al., 2010), and the secreted Wnt antagonist Notum (Zhang et al., 2015). We therefore chose to further investigate involvement of the Wnt pathway in GAER signalling by spatially validating the expression of these genes, using the most highly expressed isoforms for mRNA *in situ* hybridization by chain reaction (HCR) probe set design.

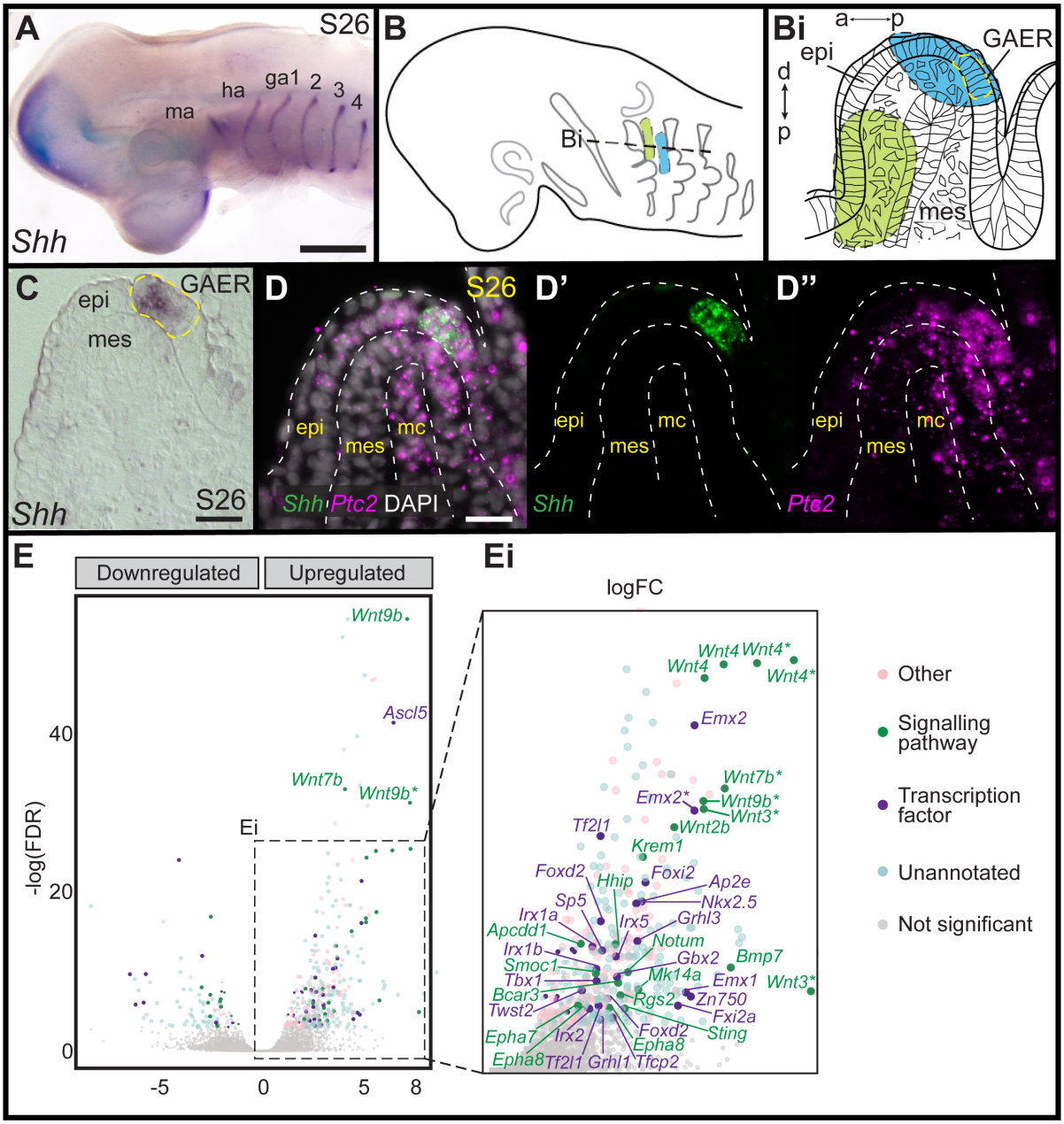

Figure 2: Differential gene expression analysis of GAER and non-GAER gill arch tissues in S26 skate embryos. (A) *Shh* is expressed in the gill arch epithelial ridge (GAER) of the hyoid and first four gill arches of skate embryos. **(B)** Schematic of dissection from gill arch 1 of **(B^{i})** the non-GAER region (control, green) and the GAER region (blue, with GAER location indicated by yellow dashed outline), as guided by (**C**) mRNA *in situ* hybridisation for *Shh* on paraffin section. **(D)** The dissected GAER region includes the *Shh*-expressing GAER, as well as adjacent Shh-responsive (i.e., *Ptc2*+) tissues, as indicated by multiplexed mRNA *in situ* hybridisation by chain reaction (HCR) for *Shh* and *Ptc2* on paraffin section. (**E, E^{i}**) Volcano plot illustrating differential

gene expression between GAER and non-GAER tissues. Genes with >2 logFC and <0.05 false discovery rate (FDR) are highlighted and assigned functional category using colour coding as per key. Genes with >2 logFC are shown in larger point size. Signalling molecules and transcription factors with >2 logFC and <0.05 FDR are labelled (* denotes manual annotation of sequence). Differential expression was determined using edgeR with a general linear model and likelihood ratio test, corrected for multiple testing using the Benjamin-Hochberg method to control the FDR. a–p indicates anterior–posterior axis, p–d indicates proximo–distal axis. epi: epithelium, ga1-4: gill arches 1-4, ha: hyoid arch, ma: mandibular arch, mes: mesenchyme. Scale bars; A: 500μm C-D: 50μm.

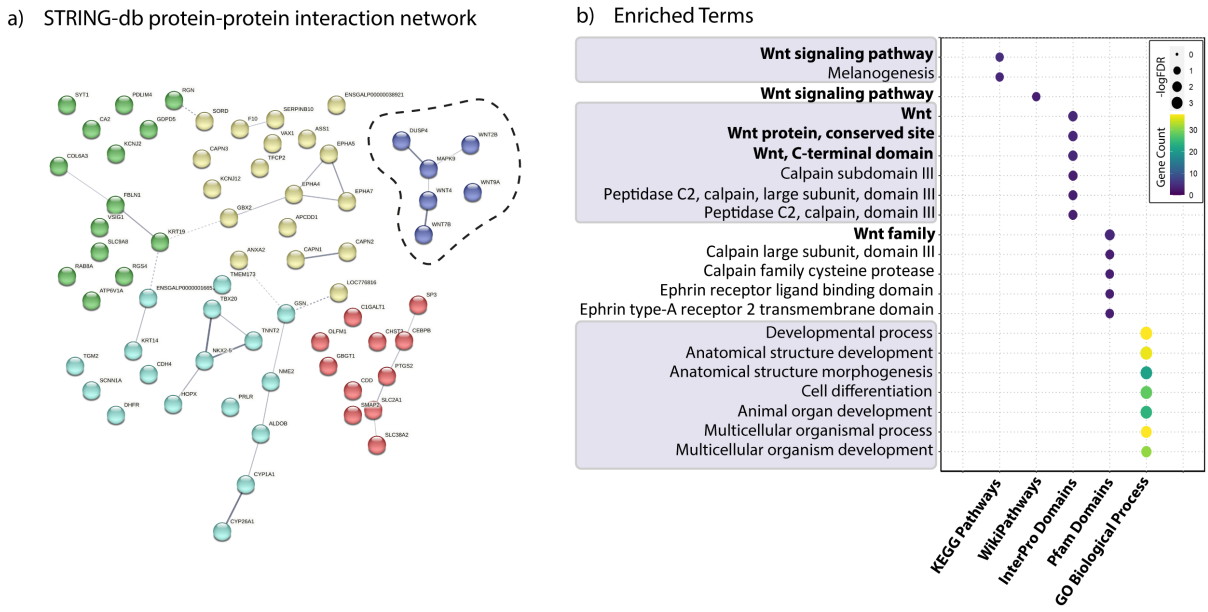

Figure 2 Supplement 1: Genes significantly upregulated in GAER vs. non-GAER gill arch tissues in S26 skate embryos. (A) All significantly upregulated genes (logFC >2, FDR <0.05) tested for interaction using STRING db v11.5, with cluster of genes encoding Wnt signalling components highlighted. **(B)** Most significantly enriched terms in GAER region tissues (GO process, KEGG Pathway, InterPro, Pfam and WikiPathway screened).

220 To characterise expression of genes encoding Wnt ligands relative to *Shh* expression
221 in the GAER, we used multiplexed ISH by HCR to visualise transcript localisation in
222 sections of S26 skate gill arches. We found that while *Wnt7b* was co-expressed
223 with *Shh* in the cells of the GAER (Fig. 3A), *Wnt2b*, *Wnt3*, *Wnt4* and *Wnt9b* (Fig. 3B–
224 E) were all expressed predominantly in the epithelium immediately adjacent to the
225 GAER. We next examined the expression of the Wnt signalling downstream target
226 genes (Fig. 4) using *Shh* or *Wnt7b* as a marker for the GAER. We found
227 that *Apcdd1* was expressed in the GAER and anterior–distal mesenchyme (Fig.
228 4A), *Notum* in the anterior–distal mesenchyme (Fig. 4B) and *Kremen1* in the anterior
229 (GAER-adjacent) epithelium (Fig. 4C). Finally, broad transcription of *Axin2* throughout
230 distal gill arch tissues (Fig. 4D) indicates that Wnt signalling within this territory is
231 occurring through the canonical/β-catenin pathway (Lustig et al., 2002). While these
232 findings do not allow us to attribute expression of specific transcriptional readouts to
233 signalling by particular Wnt ligands, our spatial expression data nevertheless indicate
234 that some Wnt signals emanating from the GAER or GAER-adjacent epithelium are
235 transduced preferentially within the anterior arch environment, in a pattern that is
236 largely complimentary to the posterior epithelial and mesenchymal transduction of Shh
237 signals from the GAER.
238
239 **Wnt and Shh expression at the ectoderm-endoderm interface of skate gill arches**
240 The epithelium of vertebrate pharyngeal arches derives from both ectoderm and
241 endoderm, but the specific germ layer origin of the GAER of cartilaginous fishes
242 (endoderm vs. ectoderm) is not known. In the skate, *Shh* is initially expressed
243 broadly in the anterior endodermal epithelium of each pharyngeal pouch, which
244 subsequently gives rise to the posterior endodermal epithelium of each pharyngeal
245 arch (Gillis and Tidswell, 2017). To test whether the GAER derives from this initially
246 broad endodermal *Shh* expression domain, we labelled the pharyngeal endoderm of
247 early skate embryos by microinjecting the lipophilic dye CM-DiI into the pharyngeal
248 cavity at stage S18. At this stage, the pharyngeal pouches have not yet fused with
249 the overlying surface ectoderm, allowing for specific CM-DiI labelling of pharyngeal
250 endodermal epithelium (Fig. 5A,B). Injected embryos were then grown to S25–S29,
251 by which time the GAER of the hyoid and gill arches is detectable by expression of
252 *Shh* (Fig. 5C).
253

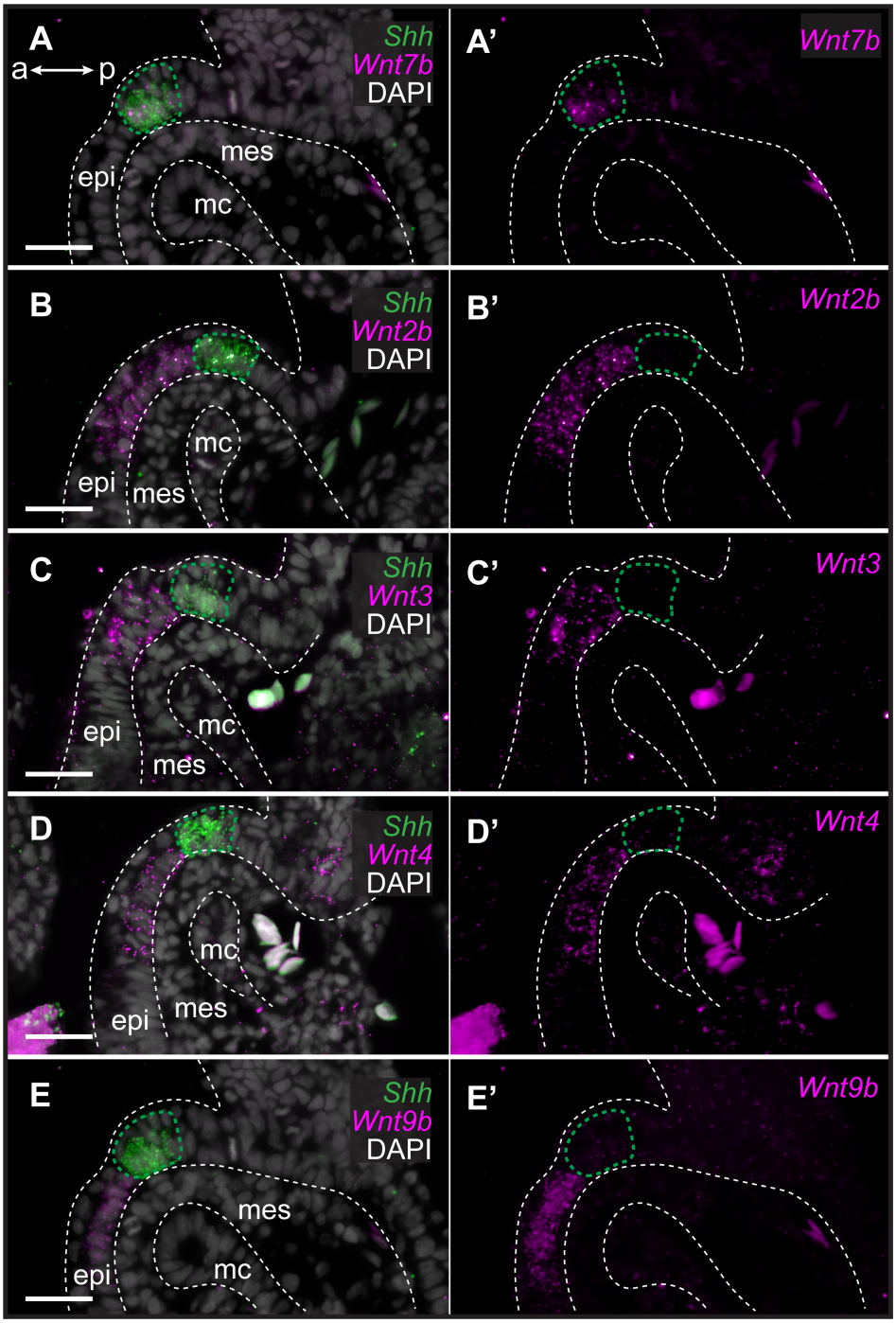

Figure 3: Genes encoding Wnt ligands are expressed in and around the GAER in skate. In S26 skates, (**A, A'**) *Wnt7b* is co-expressed with *Shh* in the GAER. (**B)** *Wnt2b,* **(C)** *Wnt3*, **(D)** *Wnt4* and **(E)** *Wnt9b* are predominantly expressed in the epithelium immediately adjacent the GAER. For ease of visualisation in **A'–E'**, *Shh* expression is not shown but GAER cells are outlined with a green dashed line. Arch tissues are outlined with white dashed lines. a–p indicates anterior–posterior axis. epi: epithelium, mes: mesenchyme, mc: mesodermal core. Scale bar: 50μm.

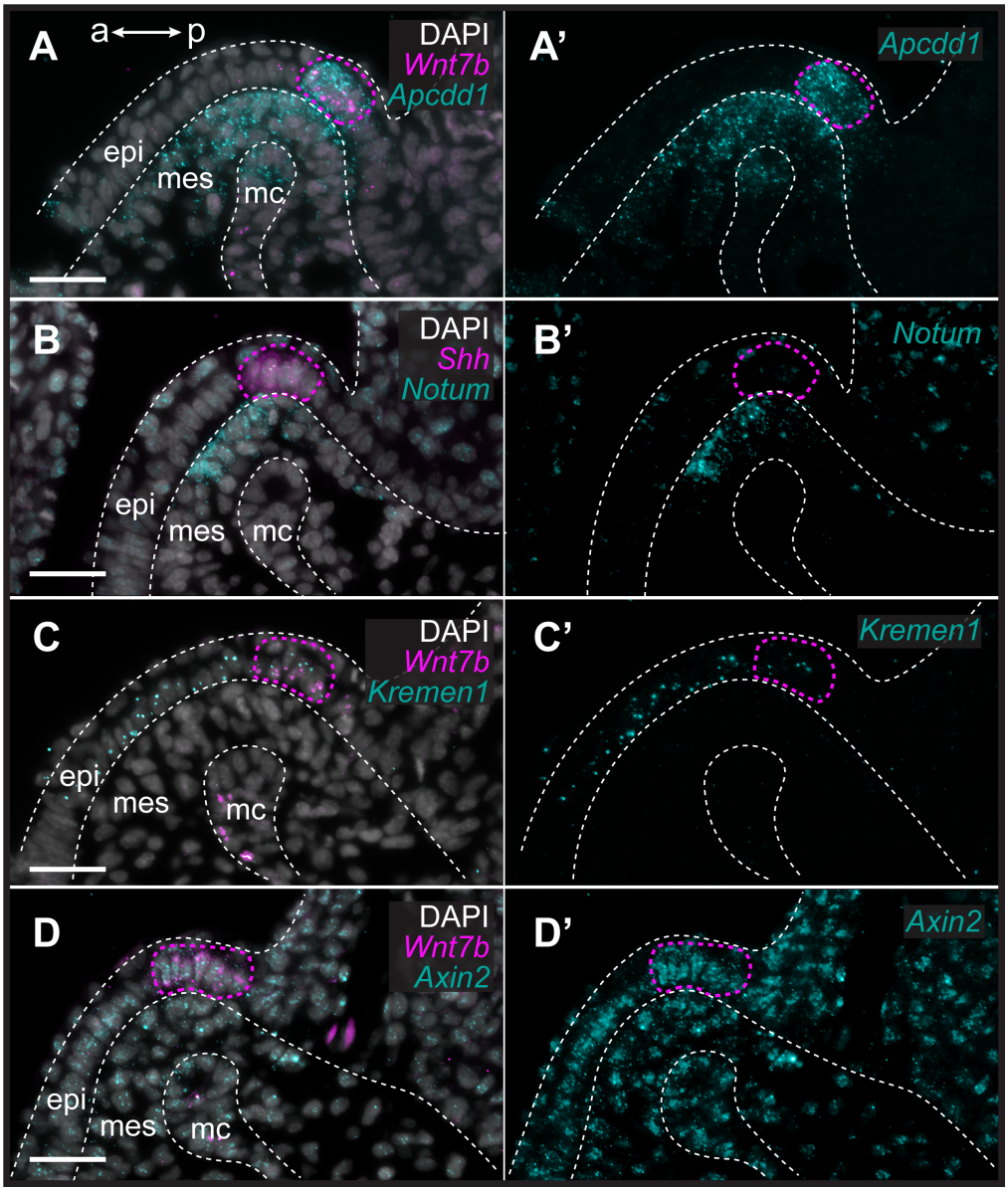

Figure 4: Transduction of canonical Wnt signalling in the anterior gill arch territory in skate. In S26 skates, (**A, A'**) *Apcdd1* is expressed in the GAER and in the anterior–distal mesenchyme underlying the GAER. (**B**) *Notum* is expressed in anterior–distal arch mesenchyme. (**C**) *Kremen1* is expressed in the GAER and in GAER-adjacent epithelium. (**D**) Broad *Axin2* expression in the vicinity of *Wnt*-expressing epithelium indicates signalling through the canonical Wnt signalling pathway. ISH by HCR for *Shh* or *Wnt7b* was performed alongside each gene of interest as a marker of the GAER (outlined with magenta dashed line). a–p indicates anterior–posterior axis. epi: epithelium, mes: mesenchyme, mc: mesodermal core. Scale bar: 50μm.

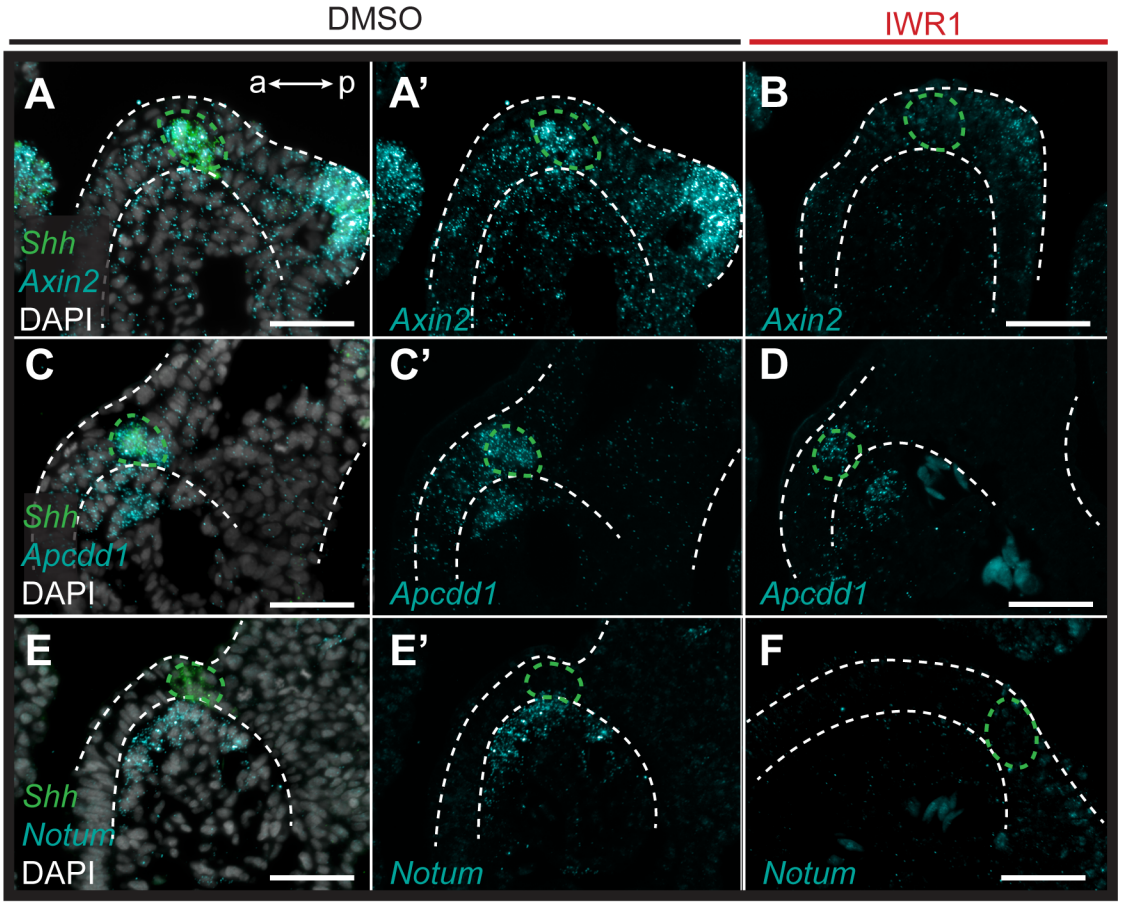

Figure 4 Supplement 1: Pharmacological inhibition of Wnt signalling in skate leads to downregulation of Wnt pathway genes. ISH by HCR was performed on sections of S26 skate embryos treated for 72hrs with either DMSO (control) or the canonical Wnt inhibitor IWR1. *Shh* was performed alongside each gene of interest as a marker of the GAER. (**A–A'**) *Axin2* is broadly expressed throughout the distal arch epithelium and mesenchyme in control embryos, with particularly strong expression in the cells of the GAER and in developing gill buds. (**B**) *Axin2* expression is substantially depressed with IWR1 treatment. (**C–C'**) *Apcdd1* is expressed in the cells of the GAER, and within anterior–distal mesenchyme in control embryos, and (**D**) both of these expression domains are reduced with IWR1 treatment. (**E–E'**) *Notum* is expressed within anterior-distal arch mesenchyme in control embryos, and (**F**) expression is completely lost in the anterior-distal arch mesenchyme with IWR1 treatment. All images are representative of experiments performed in triplicate. For ease of visualisation in (**A', B, C', D, E', F**) *Shh* expression is not shown but GAER cells are outlined with green dashed lines and arch tissues are outlined with white dashed lines. a–p indicates anterior–posterior axis in all panels. Scale bar: 50 μm.

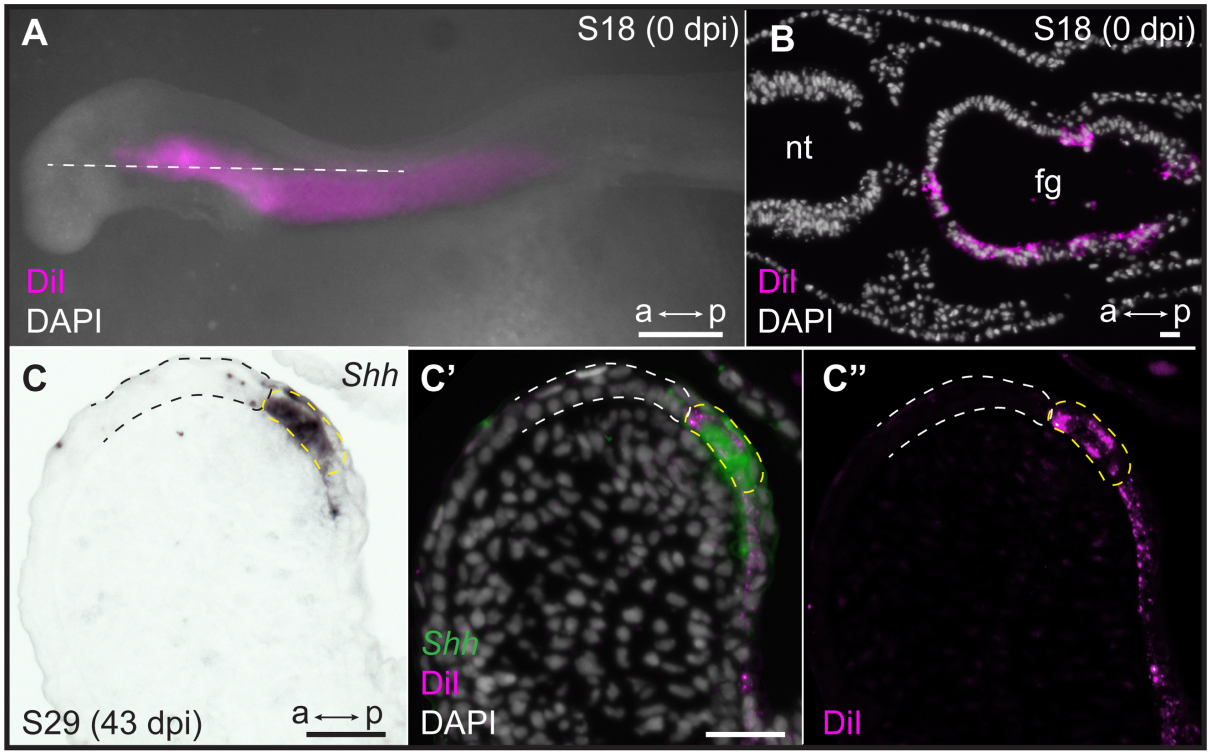

Figure 5: Endodermal origin of the skate GAER. (**A**) Microinjection of CM-DiI into the pharyngeal cavity of skate embryos at S18 results in (**B**) specific labelling of the pharyngeal endoderm. (**C**) *Shh* is a marker of the GAER (dashed yellow line) in CM-DiI-labelled embryos, and (**C', C''**) co-localisation of CM-DiI and *Shh* expression indicates that the cells of the GAER are of endodermal origin. Dashed white outline demarcates GAER-adjacent (ectodermal) epithelium, which is never labelled with CM-DiI. (**C**), (**C'**), and (**C''**) are the same section, imaged sequentially for *Shh* expression and CM-DiI. a–p indicates anterior–posterior axis. dpi: days post-injection, fg: foregut, nt: neural tube. Scale bars; A: 500μm, B–C: 40μm.

315 Of 29 embryos analysed, all retained some CM-DiI label within the endodermal lining
316 of the pharyngeal arches. In 8/29 embryos, we recovered CM-DiI labelling up to and
317 including the *Shh*-expressing cells of the GAER in one or more pharyngeal arches
318 (Fig. 5C), indicating endodermal origin of these cells. The remaining 21 embryos did
319 not have sufficient labelling of pharyngeal epithelia to inform the origin of the GAER
320 (likely due to label dilution during the long incubation time between injection and
321 analysis). Importantly, however, no CM-DiI labelling was ever observed in epithelial
322 cells immediately anterior to the GAER, suggesting that this epithelium is of
323 ectodermal origin. Together, these observations indicate that the GAER is of
324 endodermal origin and arises at the ectoderm–endoderm interface during pharyngeal
325 arch development, and that the *Wnt*-expressing epithelium immediately anterior to
326 the GAER derives from the ectoderm.
327
328 **Wnt signalling suppresses GAER Shh signal transduction in the anterior gill**
329 **arch**
330 To explore the function of Wnt signalling during skate pharyngeal arch development,
331 we inhibited canonical Wnt signalling in skate embryos using IWR1, a small molecule
332 tankyrase inhibitor that antagonises Wnt signalling by stabilising the Axin/β-catenin
333 destruction complex (Lu et al., 2009, Kulak et al., 2015). Briefly, skate embryos were
334 maintained in a bath of 50μM IWR1 or vehicle-only control (DMSO) in seawater from
335 S25 for 72h to assess gene expression changes in response to drug treatment (Fig. 4
336 Supplement 1), or for 6–8 weeks (until S31/32) to assess effects of Wnt signalling
337 inhibition on gill arch skeletal patterning, with replacement of drug- or control-seawater
338 every 48h. IWR1-treated embryos showed a marked reduction in the expression of
339 *Axin2* throughout their gill arches (Fig. 6A–B), as well as a reduction in the expression
340 of *Apcdd1* in the GAER and anterior–distal gill arch mesenchyme (Fig. 6C–D) and a
341 complete loss of *Notum* expression in anterior–distal gill arch mesenchyme (Fig. 6E–
342 F). These findings indicate that our drug treatment effectively supressed canonical
343 Wnt signalling from the GAER and GAER-adjacent epithelium, including those signals
344 transduced asymmetrically in the anterior gill arch environment.
345
346 Shh is a pro-chondrogenic signal from the GAER in skate gill arches (Gillis et al.,
347 2009b), and this signal is transduced asymmetrically with the posterior gill arch

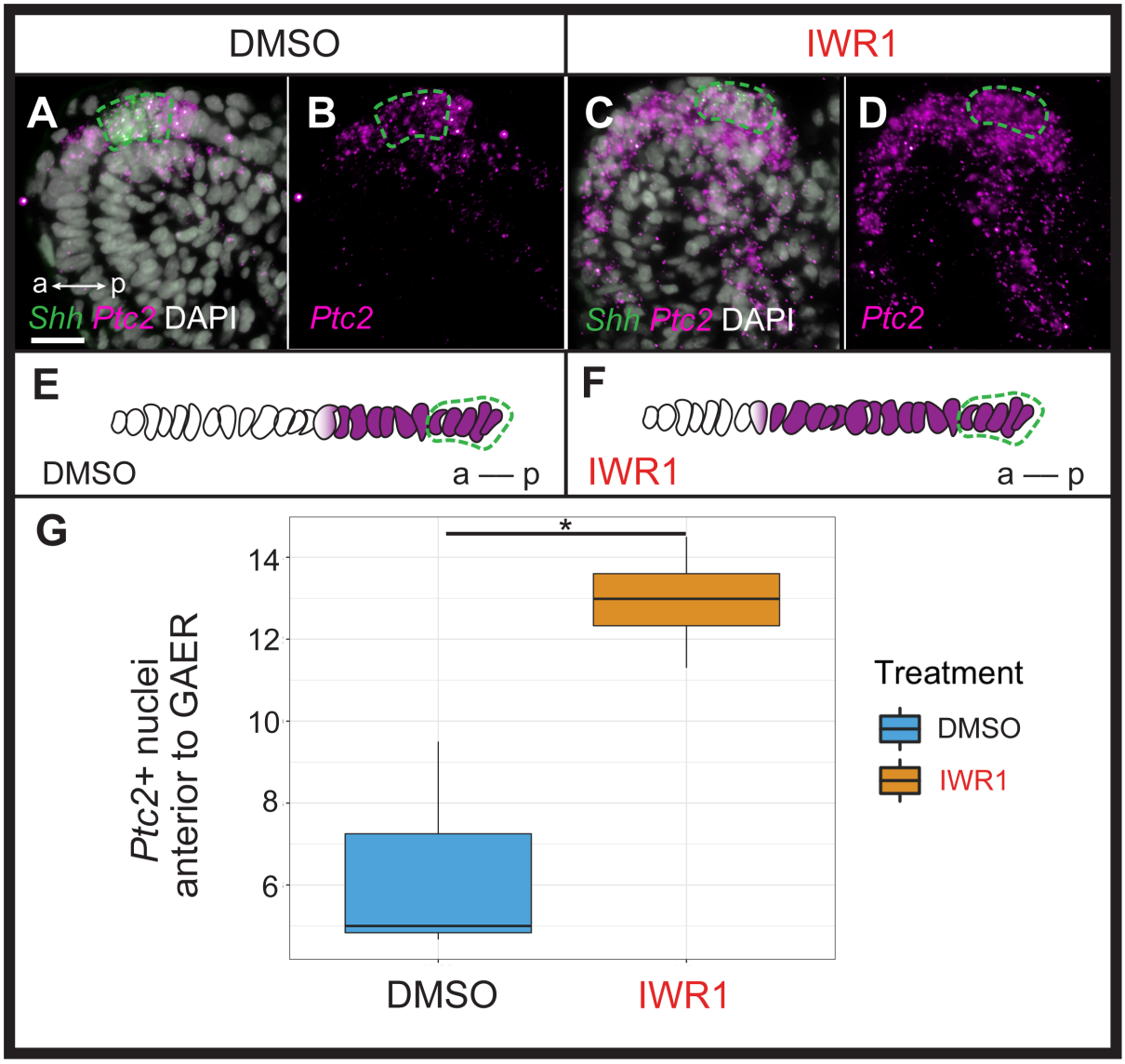

Figure 6: Wnt signalling restricts transduction of GAER Shh signalling to the posterior gill arch environment. ISH by HCR on sections of skate embryos treated for 72 hours with (**A,B**) DMSO or (**C,D**) IWR1 shows no difference in *Shh* expression but an expansion of *Ptc2* expression within the epithelium anterior to the *Shh*-expressing GAER. **(E)** Schematic illustration of the mean number of *Ptc2*+ nuclei anterior to the GAER in DMSO control (n=3 embryos; mean = 6.3 cells) or (**F**) IWR1 treated (n=4 embryos; mean = 12.94 cells) embryos, using the mean cell count of two or three sections at equivalent positions in the gill arch from each embryo. (**G**) We find a significant increase in *Ptc2*+ nuclei in the epithelium anterior to the GAER in IWR1-treated embryos compared to control (P= 0.036; t test, t= -3.87, df= 2.74). In **A–F**, *Shh* expression is indicated by green dashed line. Images in **A–D** taken using identical exposure settings. a–p indicates anterior–posterior axis. Scale bar: 20 μm.

362 environment (Gillis and Hall, 2016, and see above). To test whether anteriorly
363 transduced Wnt signalling may act to restrict Shh signal transduction to the posterior
364 gill arch, we examined expression of *Shh* and *Ptc2* in skate embryos 72h after the
365 onset of IWR1 treatment. While we observed no noticeable change in the expression
366 of *Shh* or in the spatial distribution of *Ptc2* transcripts in gill arch mesenchyme with
367 IWR1 treatment, we did note a qualitative increase in *Ptc2* expression within the
368 normal mesenchymal domain, and a clear anterior expansion of *Ptc2* expression
369 within the epithelium adjacent to the GAER. To quantify this epithelial expansion, we
370 compared the mean number of *Ptc2*+ nuclei anterior to the *Shh*-expressing GAER
371 (using DAPI staining and counted manually) across two or three sections at equivalent
372 positions in DMSO control (n=3) or IWR1 (n=4) treated embryos and found a
373 significant anterior expansion of *Ptc2* expression within the epithelium adjacent to the
374 GAER in IWR1 treated embryos (p= 0.036). This points to a role for GAER-adjacent
375 Wnt signalling in restricting the transduction of pro-chondrogenic Shh signalling in the
376 anterior gill arch territory in skate.
377
378 **Wnt signalling inhibits branchial ray development in the anterior gill arch**
379 **environment**
380 Finally, to test for an effect of Wnt inhibition on the gill arch skeleton, we reared skate
381 embryos in DMSO control seawater or IWR1 from S25–S31/32 (Fig. 7). IWR1-treated
382 embryos had several distinct phenotypic changes, including a smaller size, a loss of
383 gill filaments and disrupted fin morphology (the latter consistent with previous findings
384 of Nakamura et al. 2015 – Fig. 7A-B). We specifically investigated the impact of IWR1
385 treatment on gill arch skeletal morphology. The skate hyoid and gill arch skeleton
386 include branchial rays that articulate exclusively with the posterior margin of the gill
387 arch cartilages (Gillis et al., 2009a – see also Fig. 1). These rays also invariably
388 develop on the posterior side of the interbranchial muscle plate – a histologically and
389 molecularly distinct derivative of the paraxial mesodermal core that extends down the
390 middle of each pharyngeal arch (Daniel, 1934; Graham, 2008; Hirschberger et al.,
391 2021). Skate embryos reared in DMSO control seawater showed no gill arch skeletal
392 defects (n=4 embryos; Fig. 7Ai), while embryos reared in IWR1 seawater possessed
393 conspicuous ectopic branchial rays in the anterior gill arch territory (n= 7/8 embryos;
394 Fig. 7Bi). These ectopic branchial rays occurred along the entire dorsoventral axis of
395 the arch and ranged from short cartilage rods located in the anterior–distal gill arch to

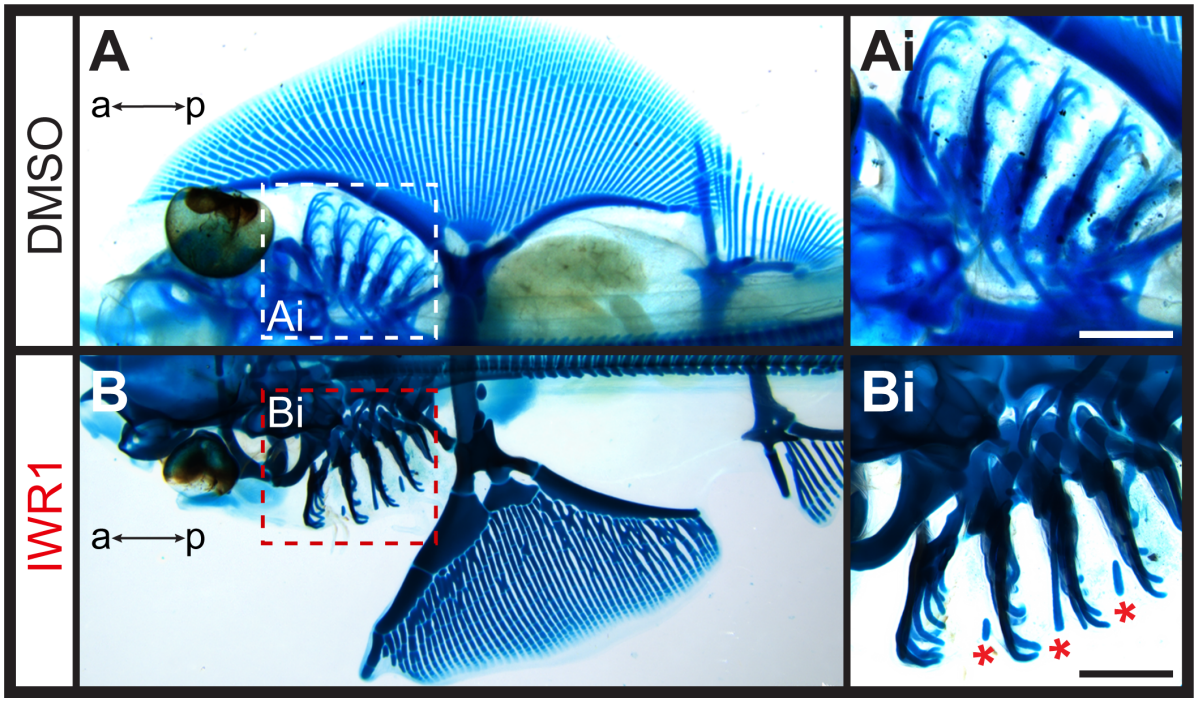

Figure 7: Ectopic branchial ray formation upon inhibition of Wnt signalling. (A) In control (DMSO) skate embryos, branchial rays (magnified in **Ai**) articulate exclusively with the posterior margin of the gill arches. **(B)** Embryos reared from S25 to S31/32 in the Wnt inhibitor IWR1 possessed ectopic branchial rays (magnified in **Bi**) that were embedded within connective tissue of the anterior gill arch (ectopic rays present in n=7/8 embryos examined; indicated by red asterisk). a–p indicates anterior–posterior axis. Scale bars: 500 μm.

417 nearly full-length branchial rays that extended much of the way toward the gill arch
418 cartilages. In section, normal branchial rays of skate embryos reared in DMSO control
419 seawater always developed on the posterior side of the mesodermally-derived
420 interbranchial muscle plate of each gill arch: this was evident from histochemical
421 staining and from HCR for the chondrocyte markers *Sox9* and *Col2a1* (Fig. 8A-B).
422 Conversely, in skate embryos reared in IWR1 seawater, ectopic branchial rays were
423 consistently located anterior to the interbranchial muscle plate (Fig. 8C-D). The
424 induction of ectopic branchial rays with IWR1 treatment suggests that Wnt signalling
425 contributes to the maintenance of anteroposterior polarity of the skate gill arch
426 skeleton by repressing chondrogenesis in the anterior gill arch and may do so by
427 restricting transduction of GAER Shh signalling to the posterior gill arch territory.
428
429
430
431
432
433
434
435
436
437
438
439
440
441
442

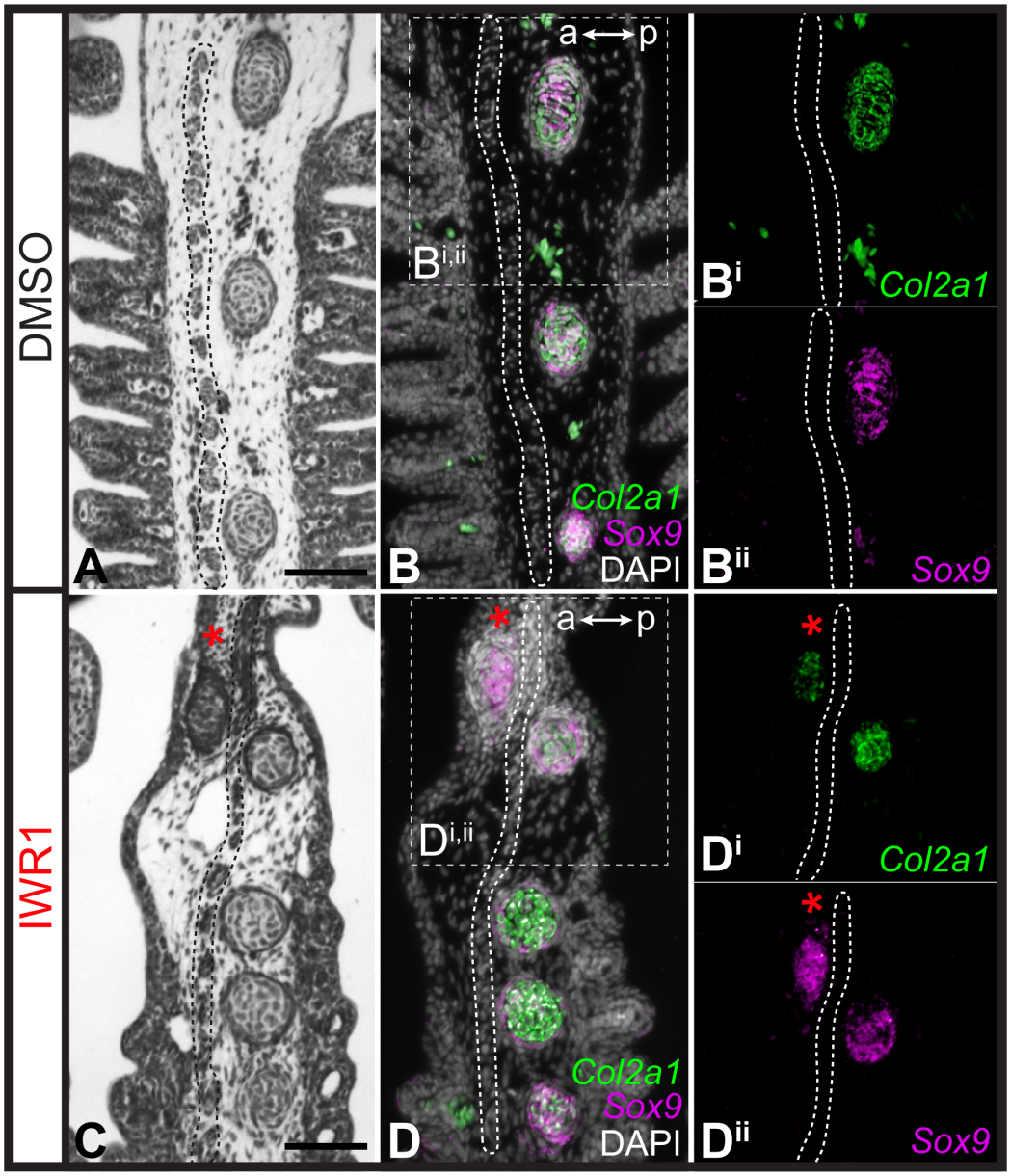

443

444

445 **Figure 8: Repression of cartilage development in the anterior gill arch by Wnt**
446 **signalling. (A)** Section through the gill arch of a control (DMSO) S31 skate embryo,
447 showing that branchial rays develop exclusively on the posterior side of the
448 interbranchial muscle plate, as is evident from histochemical staining and **(B, Bi, Bii)**
449 ISH by HCR for the chondrocyte markers *Sox9* and *Cola2a1*. **(C)** Section through the
450 gill arch of a S31 embryos reared in the canonical Wnt inhibitor IWR1 reveals that
451 ectopic branchial rays form anterior to the interbranchial muscle plate, as evident from
452 histological analysis and **(D, Di, Dii)** ISH by HCR for *Sox9* and *Col2a1*. Red asterisks
453 indicate ectopic branchial rays, and interbranchial muscle plate is outlined with a
454 dashed line. a–p indicates anterior–posterior axis. Scale bars: 50 μm.

455 # Discussion

456

457 The molecular mechanisms governing spatial regulation of cell fate decisions are
458 crucial to the establishment and maintenance of anatomical polarity within
459 developing tissues and organs. Here, we show that the GAER signalling centre that
460 forms on the hyoid and gill arches of cartilaginous fishes is of endodermal origin,
461 arising precisely at the boundary of surface ectoderm and pharyngeal endoderm,
462 and that pro-chondrogenic Shh signals from the GAER are transduced preferentially
463 within the posterior gill arch environment. We further show that the ectoderm
464 immediately anterior and adjacent to the GAER is a signalling centre that expresses
465 several Wnt family genes, and that Wnt signals from this centre are transduced
466 preferentially in the anterior arch environment. Pharmacological inhibition of
467 canonical Wnt signalling in skate embryos leads to an expansion of Shh signal
468 transduction within the anterior territory of the gill arch, and to the formation of
469 ectopic anterior branchial ray cartilage. These findings suggest that Wnt–Shh
470 signalling antagonism at the pharyngeal ectodermal–endodermal tissue boundary is
471 a key molecular regulator of cell fate determination and anatomical polarity with the
472 developing gill arch skeleton of the skate (Fig. 9).

473

474 Previous analyses have reported the expression of several Wnt genes in developing
475 craniofacial tissues of bony vertebrates (Summerhurst et al., 2008), including
476 expression of *WNT2B* and *WNT9B* in the pharyngeal arch ectoderm of the chick
477 (Geetha-Loganathan et al., 2009), *Wnt9b* in the first and second pharyngeal arches in
478 zebrafish (Jezewski et al., 2008), *Wnt4a* in zebrafish pharyngeal ectoderm (Choe et
479 al., 2013), and Wnt9a and Wnt5b in zebrafish oral epithelium (Dougherty et al., 2013;
480 Rochard et al., 2016). While β-catenin-independent (i.e., non-canonical) Wnt signalling
481 plays a crucial role in epithelial remodelling during the early formation of pharyngeal
482 endodermal pouches in zebrafish (Choe et al., 2013) and in maturation and
483 morphogenesis of the zebrafish oropharyngeal skeleton (Rochard et al., 2016; Ling et
484 al., 2017), canonical Wnt signalling has been implicated in patterning of the pharyngeal
485 arch-derived skeleton in multiple taxa. Blocking canonical Wnt signalling causes
486 disrupted facial cartilage formation, including reductions of Meckel's and ceratohyal
487 cartilages in zebrafish (Alexander et al., 2014) and loss of ectodermal canonical Wnt

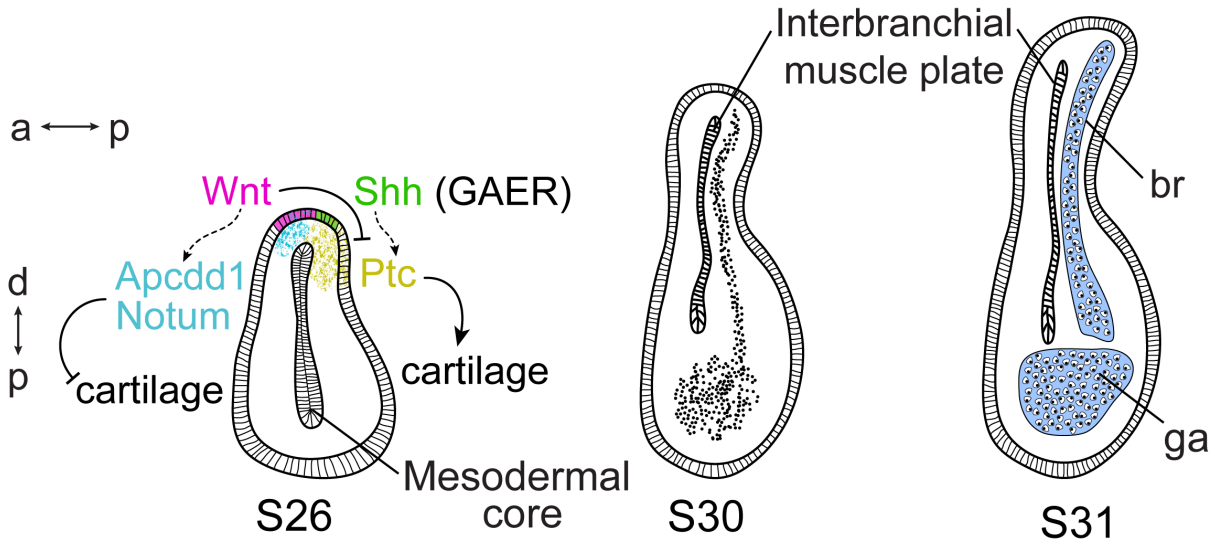

Figure 9: Wnt and Shh signalling and cell fate determination in skate gill arches. Shh signalling from the endodermally-derived GAER is transduced within the posterior-distal gill arch (ga) environment, where it promotes the differentiation of cartilaginous branchial rays (br). Wnt signals from ectoderm adjacent to the GAER are transduced within the anterior–distal gill arch environment, where they repress Shh signal transduction and inhibit cartilage formation in the anterior gill arch. a–p indicates the anterior-posterior axis and p–d indicates the proximo–distal axis.

512 signalling in mouse causes loss of facial bones with hypoplasia of all facial
513 prominences (Reid et al., 2011). Furthermore, in mouse and human, cleft palate
514 phenotypes may arise as a consequence of mutations in *Wnt3* and *Wnt9b* (Niemann
515 et al., 2004, Juriloff et al., 2006), and perturbation of Wnt/β-catenin signalling has been
516 implicated in CATSHL syndrome, a human developmental disorder involving
517 craniofacial bone malformation and mispatterning of the pharyngeal arches (Sun et
518 al., 2020). Our finding of a role for canonical Wnt signalling in patterning the gill arch
519 skeleton of skate may therefore reflect broadly conserved roles for this pathway in
520 pharyngeal skeletal development across jawed vertebrates, though with the skate's
521 possession of branchial rays offering a unique anatomical readout of anterior–
522 posterior polarity defects that arise within the pharyngeal arch-derived skeleton in
523 response to perturbations.
524
525 Our findings are also consistent with previously reported complex and context-
526 dependent roles for Wnt signalling in the regulation of cell fate determination events
527 during vertebrate skeletogenesis. In some instances, Wnt signalling functions to
528 promote skeletogenesis: for example, in chick, misexpression of *WNT5A*/*5B* promotes
529 early chondrogenesis of limb bud mesenchyme *in vitro* and delays the terminal
530 differentiation of growth plate chondrocytes *in vivo* (Church et al., 2002), and in mouse,
531 canonical WNT signalling from cranial ectoderm induces specification of osteoblast
532 progenitors of cranial dermal bone within underlying mesenchyme (Goodnough et al.,
533 2016). However, in other contexts, Wnt signalling functions to inhibit chondrogenic
534 differentiation or homeostasis. In chick, signalling through WNT3, 4, 7A, 14 or FZ7
535 have all been shown to inhibit chondrogenesis *in vitro* or *in vivo* (Rudnicki and Brown,
536 1997), while in mouse conditionally induced haploinsufficiency of the gene encoding
537 the β-catenin degradation complex component APC (i.e., activation of canonical Wnt
538 signalling) results in loss of resting zone chondrocytes and their clonal progeny in
539 developing growth plates (Hallett et al., 2021). In the limb bud, genes encoding WNT
540 ligands are expressed in the ectoderm (Kengaku et al., 1998, Parr et al., 1993,
541 Geetha-Loganathan et al., 2005; Summerhurst et al., 2008), where they function
542 synergistically with FGF signalling from the apical ectoderm ridge to inhibit
543 chondrogenesis of limb bud mesenchyme and to promote soft connective tissue fates
544 (ten Berge et al., 2008). Downstream effectors of Wnt signalling are expressed out-of-
545 phase with Sox9+ digit progenitors in the mouse limb bud, with Wnt signalling

546 functioning to repress digit chondrogenesis as part of a Turing-like mechanism that
547 underlies periodic patterning of the distal limb endoskeleton (Raspopovic et al., 2014).
548 Our findings therefore demonstrate a striking parallel between developing skate gill
549 arches and tetrapod limb buds, with Wnt signals emanating from ridge-adjacent
550 epithelia functioning to inhibit chondrogenic differentiation, thereby ensuring
551 differentiation of cartilaginous appendages in a spatially controlled manner.
552
553 We have previously shown that Shh signalling from the GAER is required for branchial
554 ray chondrogenesis in skate (Gillis and Hall, 2016), and that the application of
555 exogenous SHH protein to the anterior gill arch is sufficient to induce ectopic branchial
556 rays (Gillis et al., 2009b). However, it is unclear whether Shh from the GAER is a direct
557 inducer of chondrogenesis in the posterior arch mesenchyme, or rather induces
558 chondrogenesis indirectly, via a secondary signal (i.e., emanating from the Shh-
559 responsive epithelium or mesenchyme). We have observed that inhibition of Wnt
560 signalling in skate embryos has no effect on the expression of *Shh* in the GAER, but
561 rather results in an anterior expansion of Shh signal transduction in the gill arch
562 ectoderm, which in turn, correlates with ectopic chondrogenesis in the anterior gill
563 arch. This observation indicates that the pro-chondrogenic influence of GAER Shh
564 signalling may be indirect, occurring via a secondary Shh-depending epithelial signal
565 whose expression is typically posteriorly restricted by Wnt signalling from GAER-
566 adjacent ectoderm. The Shh and Wnt signalling pathways share multiple downstream
567 components (reviewed in Ding and Wang, 2017). For example, components of the
568 canonical Wnt signalling pathway can positively regulate Shh signalling via GSK3β,
569 by phosphorylating the downstream component SUFU and promoting the release of
570 SUFU from Gli (Takenaka et al., 2007), and by β-catenin affecting Gli1 transcriptional
571 activity via TCF/LEF (Maeda et al., 2006). It has also been found that Gli3 may function
572 as a downstream effector of the Wnt pathway, and that Wnt signalling represses Shh
573 activity in the dorsal neural tube through the regulation of *Gli3* expression (Alvarez-
574 Medina et al., 2008). Finally, the Shh signalling pathway may regulate Wnt signalling
575 through Gli1 and Gli2, with these factors positively regulating the expression of the
576 secreted Wnt inhibitor *frizzled-related protein-1* (*sFRP-1*) (He et al., 2006). These
577 mechanisms, or others, could account for the apparent cross regulation between Wnt
578 and Shh signalling that we have observed during growth and patterning of skate
579 pharyngeal arches.

Finally, it remains to be determined whether antagonistic ectodermal Wnt and endodermal Shh signalling is a derived mechanism of cell fate determination and pharyngeal skeletal patterning in cartilaginous fishes, or a conserved feature of the pharyngeal arches of jawed vertebrates. In bony vertebrates, a Shh-expressing posterior endodermal margin (PEM) promotes proliferative expansion of the second (hyoid) pharyngeal arch (Wall and Hogan, 1995; Richardson et al., 2012; Rees and Gillis, 2022). In bony fishes, the hyoid arch gives rise to an operculum that is supported by a series of dermal bones, and this operculum functions as a protective cover for the gills that arise from the posterior pharyngeal arches, whereas in amniotes, the hyoid arch expands caudally and ultimately fuses with the cardiac eminence to enclose the cervical sinus and close the surface of the neck (Richardson et al., 2012). Amniotes lack homologues of the opercular series of bony fishes or the cartilaginous branchial rays of cartilaginous fishes, respectively, but fossil evidence points the operculate condition of bony fishes as ancestral for jawed vertebrates (Dearden et al., 2019). Whether juxtaposed Wnt- and Shh-expressing epithelia influence fate determination (e.g., dermal bone vs. connective tissue) and patterning within the opercular series of bony fishes is not known. Further comparative work between bony and cartilaginous fishes with disparate pharyngeal skeletal architectures and tissue compositions will permit inference of ancestral functions and interactions of epithelial signals during vertebrate pharyngeal arch skeletal development.

610 # Materials and Methods

611

612 **Embryo harvesting**

613 Skate (*L. erinacea)* embryos were obtained from the Marine Resources Center at the
614 Marine Biological Laboratory in Woods Hole, MA, U.S.A., were reared as described in
615 Gillis *et al.* (2012) and staged according to Ballard *et al.* (1993) and Maxwell et al.
616 (2008). Skate embryos were euthanised with an overdose of MS-222 (1g/L in
617 seawater), and all embryos were fixed in 4% paraformaldehyde (Thermofisher) as per
618 Gillis *et al.* (2012).

619

620 **Sectioning and histochemical staining**

621 Embryos were embedded in paraffin and sectioned at 7μm as described in O'Neill et
622 al. (2007). Sectioned embryos were stained with Masson's Trichrome as per Witten
623 and Hall (2003) or Mayer's Hematoxylin and Eosin by clearing in two rinses of Histosol
624 (National Diganostics), rehydration through serial dilutions of ethanol, staining for 15
625 minutes in Mayer's Haematoxylin (Sigma), rinsing in running tap water for 20 minutes,
626 rinsing briefly in 95% ethanol, and staining in 0.1% w/v Eosin Y (Sigma) in 95% ethanol
627 for 2 minutes. Slides were then washed briefly in 95% ethanol, washed briefly with
628 100% ethanol, cleared with Histosol, and mounted with permount (Sigma).

629

630 **Lineage tracing**

631 Endodermal lineage tracing was performed by microinjection of CellTracker™ CM-DiI
632 (1,1'-dioctadecyl-3,3,3'3'-tetramethylindocarbocyanine perchlorate; Thermofisher)
633 into the pharyngeal cavity of stage (S)18 skate embryos with a pulled glass needle.
634 CM-DiI was prepared as per Gillis *et al.* (2012). Labelled embryos were then grown to
635 S25–29, euthanised, fixed, embedded, and sectioned as described above, and CM-
636 DiI localisation was assessed relative to the GAER based on mRNA *in situ*
637 hybridisation for *Shh* (see below).

638

639 **mRNA *in situ* hybridisation**

640 Chromogenic mRNA in situ hybridisation (ISH) was performed on paraffin sections
641 and in wholemount as described in O'Neill *et al*. (2007), with modifications according
642 to Gillis *et al.* (2012). An ISH probe against skate *Shh* (GenBank EF100667) was

643 generated by *in vitro* transcription using standard methods. Following ISH,
644 wholemounts were rinsed, post-fixed in 4% paraformaldehyde and graded into 75%
645 glycerol for imaging, while slides were rinsed in PBS, post-fixed in 4%
646 paraformaldehyde and coverslipped with DAPI-Fluoromount® G (SouthernBiotech).
647 Third-generation mRNA ISH by chain reaction (HCR) was performed as per the Choi
648 *et al* (2018) protocol for formaldehyde fixed, paraffin-embedded sections, with
649 modifications as per Criswell and Gillis (2020). Probes, buffers, and hairpins were
650 purchased from Molecular Instruments (Los Angeles, California, USA). HCR probe set
651 lot numbers are as follows: skate *Shh* (Lot PRA753), *Ptc2* (Lot PRA754), *Wnt2b* (Lot
652 PRE300), *Wnt3* (Lot PRG814), *Wnt4* (Lot PRE301), *Wnt7b* (Lot PRE302), *Wnt9b* (Lot
653 PRE303), *Notum* (Lot PRG817), *Kremen1* (Lot PRG816), *Axin2* (Lot PRG818),
654 *Apcdd1* (Lot PRG815), *Col2a1* (Lot PRB574) and *Sox9* (Lot PRB571). All mRNA ISH
655 experiments were replicated, at minimum, in biological triplicate.
656
657 **Pharmacological manipulations**
658 For systemic inhibition of canonical Wnt signalling, experimental and control skate
659 embryos were reared at 15°C in petri dishes containing 50μM IWR1 (Selleck
660 chemicals) in artificial seawater or artificial seawater containing an equivalent volume
661 of vehicle (DMSO) only, respectively. IWR1 has been used previously to inhibit
662 canonical Wnt signalling in skate embryos by Nakamura et al. (2015) and in shark
663 embryos by Thiery et al. (2022). For these experiments, IWR1 was diluted to working
664 concentration from a 25mM stock solution in DMSO. Skate embryos were reared in
665 IWR1- or vehicle-containing seawater from S25 until S31/32, with drug or control
666 seawater changes every 48 hours. Once embryos reached the desired stage, they
667 were euthanised, fixed and processed for wholemount skeletal preparation according
668 to the protocol of Gillis et al. (2009a) or paraffin histology as described above.
669
670 **RNA-Seq analysis of differentially expressed genes in the GAER region**
671 GAER or non-GAER ("control") regions of gill arch 1 were manually dissected from
672 skate embryos at S26 using tungsten needles and flash frozen in lysis buffer using
673 liquid nitrogen. In all cases, GAER and control sample pairs were collected from the
674 same arch within the same embryos, or from opposite arches within the same embryo.
675 RNA was extracted from each sample using the RNAaqueous®-Micro Kit. cDNA was

676 synthesised from extracted RNA according to the Smart-seq2 protocol (Picelli et al.,
677 2014) and libraries were prepared using the Nextera XT kit (Illumina). Prior to
678 sequencing, barcoded libraries were pooled in equal proportions and checked for
679 quality, insert size and quantity using Qubit 2.0, and Agilent2100. Sequencing of the
680 20 libraries generated was conducted by Novogene on an Illumina Hi-Seq-XTen
681 generating 150bp paired-end reads. The Cambridge Service for Data-Driven
682 Discovery (CSD3) high performance computer was used for cleaning, normalisation,
683 quality assessment, assembly, abundance quantification and annotation, as per
684 (Hirschberger et al., 2021). Raw reads were cleaned to remove adapter contamination
685 using Trim Galore v0.4.0 (parameters: --paired -q 20 –nextera), for quality (Phred
686 score 20) and minimum read length (149bp) using ea-utils tool fastq-mcf (parameters:
687 -q 20 -l 100) (Aronesty, 2011). Prior to assembly, all libraries were normalised using
688 Trinity v2.6.6 *in silico* read normalisation (Haas et al., 2013) (parameters: --JM 100G
689 --max_cov 75). Trinity v2.6.6 was used to assemble the normalised reads
690 (parameters: --seqType fq --max_memory 250G --CPU 50 --min_contig_length 450)
691 (Nishimura et al., 2017, Langmead et al., 2009, Marcais and Kingsford, 2011). Basic
692 Local Alignment Search Tool (BLAST) was used to compare the assembly to the
693 Uniprot protein database with an e-value cut-off of e-20 to search for sequence
694 similarity (Altschul et al., 1990). Transcript abundance was estimated using Salmon,
695 an alignment-free quantification method, via Trinity v2.6.6 utilities (Haas et al., 2013,
696 Patro et al., 2017). A matrix was built for each of the libraries of gene-level abundance
697 estimates (raw counts) using the Trinity abundance_estimates_to_matrix.pl script.
698 MDS principal component analysis was used to check for batch effects and outliers.
699 Individual embryo origin was a batch effect and so was accordingly accounted for in
700 the additive general linear model. Differentially expressed genes between control and
701 GAER tissue samples were identified using the edgeR_3.28.0 package in R version
702 3.6.2 (Robinson et al., 2010) using a generalised linear model likelihood ratio test
703 (Chen, 2008) using a false discovery rate of 5% and no log fold-change (LogFC) cut-
704 off. See supplementary information for assembly statistics, differential expression
705 analysis and all R scripts used.
706
707 Significantly upregulated genes in the S26 GAER tissue (logFC>2, FDR<0.05) were
708 extracted and annotated using blastx sequence similarity searches against the
709 Swissprot/Uniprot database (taxid: *Gallus gallus*). Annotation IDs were inputted into

710 the STRING (v11.5) webserver and tested for predicted protein-protein interactions.
711 In the protein-protein interaction analysis, line thickness was set to show confidence,
712 and a medium confidence threshold was set. The interaction network was then tested
713 for functional enrichment against a series of databases (Gene Ontology Biological
714 Process, KEGG Pathways, WikiPathways, Pfam Domains and InterPro Domains)
715 using the default whole genome as the background. Results from the functional
716 enrichment were downloaded and Rstudio (GGplot2) was used to generate dot plots
717 to visualise the most significantly enriched terms.
718
719 Differentially upregulated genes with a log-fold change over 2 were manually screened
720 for genes involved in known signalling pathways and transcription factors to generate
721 a list for candidate gene validation by ISH. Wnt family members were highly
722 upregulated in the GAER region so were validated as candidate markers for this region
723 through third-generation ISH. Transcripts for probes in skate were based on the most
724 highly expressed isoforms.
725
726 **Imaging and figure preparation**
727 Images were taken on a Zeiss Axioscope.A1 compound microscope with a Zeiss
728 colibri 7 fluorescence LED light source using a Zeiss Axiocam 305 colour or 503 mono
729 camera and ZenPro software or a Leica M165FC stereomicroscope, a Leica DFC7000
730 T camera and LAS X software. All figures were assembled using Fiji and Adobe
731 creative cloud, with some images flipped or colours inverted for clarity and consistency
732 where needed.
733
734 **Acknowledgements**
735 With thanks to Dr Kate Criswell and Dr Christine Hirschberger for advice, and to the
736 University of Cambridge Wellcome PhD Programme in Developmental Mechanisms.
737 The authors were funded by a Wellcome PhD studentship (214953/Z/18/Z) to JMR,
738 and by a Royal Society University Research Fellowship (UF130182 and
739 URF\R\191007) and Royal Society Research Grant (RG140377) to JAG.
740
741 **Data Accessibility**
742
743 All data and R scripts for analysis have been deposited on Figshare:

10.6084/m9.figshare.19615779

RNA sequencing data are available at NCBI-SRA under BioProject ID: PRJNA825354

Biosample accessions: SAMN27512544, SAMN27512545, SAMN27512546, SAMN27512547, SAMN27512548, SAMN27512549, SAMN27512550, SAMN27512551, SAMN27512552, SAMN27512553, SAMN27512554, SAMN27512555, SAMN27512556, SAMN27512557, SAMN27512558, SAMN27512559, SAMN27512560, SAMN27512561, SAMN27512562, SAMN27512563

Probes were purchased from Molecular Instruments (Los Angeles, California, USA). This included the following: for skate *Shh* (Lot PRA753), *Ptc2* (Lot PRA754), *Fgf8* (Lot PRA755), *Dusp6* (Lot PRA756), *Wnt2b* (Lot PRE300), *Wnt3* (Lot PRG814), *Wnt4* (Lot PRE301), *Wnt7b* (Lot PRE302), *Wnt9b* (Lot PRE303), Notum (Lot PRG817), *Kremen1* (Lot PRG816), *Axin2* (Lot PRG818), *Apcdd1* (Lot PRG815), *Col2a1* (Lot PRB574) and *Sox9* (Lot PRB571).

References

ALEXANDER, C., PILOTO, S., LE PABIC, P. & SCHILLING, T. F. 2014. Wnt signaling interacts with bmp and edn1 to regulate dorsal-ventral patterning and growth of the craniofacial skeleton. *PloS Genet,* 10**,** e1004479.

ALTSCHUL, S. F., GISH, W., MILLER, W., MYERS, E. W. & LIPMAN, D. J. 1990. Basic local alignment search tool. *J Mol Biol,* 215**,** 403-10.

ALVAREZ-MEDINA, R., CAYUSO, J., OKUBO, T., TAKADA, S. & MARTI, E. 2008. Wnt canonical pathway restricts graded Shh/Gli patterning activity through the regulation of Gli3 expression. *Development,* 135**,** 237-47.

ARONESTY, E. 2011. *Command-line tools for processing biological sequencing data* [Online]. Available: https://github.com/ExpressionAnalysis/ea-utils [Accessed January 2020].

BALLARD, W. W., MELLINGER, J. & LECHENAULT, H. 1993. A series of normal stages for development of Scyliorhinus canicula, the lesser spotted dogfish (Chondrichthyes: Scyliorhinidae). *Journal of Experimental Zoology,* 267**,** 318-336.

BRITO, J. M., TEILLET, M. A. & LE DOUARIN, N. M. 2006. An early role for sonic hedgehog from foregut endoderm in jaw development: ensuring neural crest cell survival. *Proc Natl Acad Sci U S A,* 103**,** 11607-12.

CHEN, Y. 2008. *edgeR: differential analysis of sequence read count data* [Online]. Available: https://www.bioconductor.org/packages/release/bioc/vignettes/edgeR/inst/doc/edgeRUsersGuide.pdf [Accessed].

CHOE, C. P., COLLAZO, A., TRINH LE, A., PAN, L., MOENS, C. B. & CRUMP, J. G. 2013. Wnt-dependent epithelial transitions drive pharyngeal pouch formation. *Dev Cell,* 24**,** 296-309.

CHOI, H. M. T., SCHWARZKOPF, M., FORNACE, M. E., ACHARYA, A., ARTAVANIS, G., STEGMAIER, J., CUNHA, A. & PIERCE, N. A. 2018. Third-generation in situ hybridization chain reaction: multiplexed, quantitative, sensitive, versatile, robust. *Development,* 145.

CHURCH, V., NOHNO, T., LINKER, C., MARCELLE, C. & FRANCIS-WEST, P. 2002. Wnt regulation of chondrocyte differentiation. *J Cell Sci,* 115**,** 4809-18.

808 COULY, G., CREUZET, S., BENNACEUR, S., VINCENT, C. & LE DOUARIN, N. M.
809 2002. Interactions between Hox-negative cephalic neural crest cells and the
810 foregut endoderm in patterning the facial skeleton in the vertebrate head.
811 *Development,* 129**,** 1061-73.
812 COULY, G. & LE DOUARIN, N. M. 1990. Head morphogenesis in embryonic avian
813 chimeras: evidence for a segmental pattern in the ectoderm corresponding to
814 the neuromeres. *Development,* 108**,** 543-58.
815 CRISWELL, K. E. & GILLIS, J. A. 2020. Resegmentation is an ancestral feature of
816 the gnathostome vertebral skeleton. *Elife,* 9.
817 DANIEL, J. F. 1934. *The elasmobranch fishes,* Berkeley,Calif., University of
818 California press.
819 DEARDEN, R. P., STOCKEY, C. & BRAZEAU, M. D. 2019. The pharynx of the
820 stem-chondrichthyan Ptomacanthus and the early evolution of the
821 gnathostome gill skeleton. *Nat Commun,* 10**,** 2050.
822 DING, M. & WANG, X. 2017. Antagonism between Hedgehog and Wnt signaling
823 pathways regulates tumorigenicity. *Oncol Lett,* 14**,** 6327-6333.
824 DOUGHERTY, M., KAMEL, G., GRIMALDI, M., GFRERER, L., SHUBINETS, V.,
825 ETHIER, R., HICKEY, G., CORNELL, R.A. & LIAO, E.C. 2013. Distinct
826 requirements for wnt9a and irf6 in extension and integration mechanisms
827 during zebrafish palate morphogenesis. *Development*, 140, 76-81.
828 GEETHA-LOGANATHAN, P., NIMMAGADDA, S., ANTONI, L., FU, K., WHITING, C.
829 J., FRANCIS-WEST, P. & RICHMAN, J. M. 2009. Expression of WNT
830 signalling pathway genes during chicken craniofacial development. *Dev Dyn,*
831 238**,** 1150-65.
832 GEETHA-LOGANATHAN, P., NIMMAGADDA, S., PROLS, F., PATEL, K., SCAAL,
833 M., HUANG, R. & CHRIST, B. 2005. Ectodermal Wnt-6 promotes Myf5-
834 dependent avian limb myogenesis. *Dev Biol,* 288**,** 221-33.
835 GILLIS, J. A., DAHN, R. D. & SHUBIN, N. H. 2009a. Shared developmental
836 mechanisms pattern the vertebrate gill arch and paired fin skeletons. *Proc*
837 *Natl Acad Sci U S A,* 106**,** 5720-4.
838 GILLIS, J. A., DAHN, R. D. & SHUBIN, N. H. 2009b. Chondrogenesis and homology
839 of the visceral skeleton in the little skate, Leucoraja erinacea (Chondrichthyes:
840 Batoidea). *J Morphol,* 270**,** 628-43.

841 GILLIS, J. A. & HALL, B. K. 2016. A shared role for sonic hedgehog signalling in
842 patterning chondrichthyan gill arch appendages and tetrapod limbs.
843 *Development,* 143**,** 1313-7.
844 GILLIS, J. A., MODRELL, M. S., NORTHCUTT, R. G., CATANIA, K. C., LUER, C. A.
845 & BAKER, C. V. 2012. Electrosensory ampullary organs are derived from
846 lateral line placodes in cartilaginous fishes. *Development,* 139**,** 3142-6.
847 GILLIS, J. A., RAWLINSON, K. A., BELL, J., LYON, W. S., BAKER, C. V. &
848 SHUBIN, N. H. 2011. Holocephalan embryos provide evidence for gill arch
849 appendage reduction and opercular evolution in cartilaginous fishes. *Proc Natl*
850 *Acad Sci U S A,* 108**,** 1507-12.
851 GILLIS, J. A. & TIDSWELL, O. R. 2017. The Origin of Vertebrate Gills. *Curr Biol,* 27**,**
852 729-732.
853 GOODNOUGH, L. H., DINUOSCIO, G. J. & ATIT, R. P. 2016. Twist1 contributes to
854 cranial bone initiation and dermal condensation by maintaining Wnt signaling
855 responsiveness. *Dev Dyn,* 245**,** 144-56.
856 GRAHAM, A. 2008. Deconstructing the pharyngeal metamere. *J Exp Zool B Mol Dev*
857 *Evol*, 310, 336-344.
858 GRAHAM, A. & SMITH, A. 2001. Patterning the pharyngeal arches. *Bioessays,* 23**,**
859 54-61.
860 GREVELLEC, A. & TUCKER, A. S. 2010. The pharyngeal pouches and clefts:
861 Development, evolution, structure and derivatives. *Semin Cell Dev Biol,* 21**,**
862 325-32.
863 HAAS, B. J., PAPANICOLAOU, A., YASSOUR, M., GRABHERR, M., BLOOD, P. D.,
864 BOWDEN, J., COUGER, M. B., ECCLES, D., LI, B., LIEBER, M.,
865 MACMANES, M. D., OTT, M., ORVIS, J., POCHET, N., STROZZI, F.,
866 WEEKS, N., WESTERMAN, R., WILLIAM, T., DEWEY, C. N., HENSCHEL,
867 R., LEDUC, R. D., FRIEDMAN, N. & REGEV, A. 2013. De novo transcript
868 sequence reconstruction from RNA-seq using the Trinity platform for
869 reference generation and analysis. *Nat Protoc,* 8**,** 1494-512.
870 HALLETT, S. A., MATSUSHITA, Y., ONO, W., SAKAGAMI, N., MIZUHASHI, K.,
871 TOKAVANICH, N., NAGATA, M., ZHOU, A., HIRAI, T., KRONENBERG, H. M.
872 & ONO, N. 2021. Chondrocytes in the resting zone of the growth plate are
873 maintained in a Wnt-inhibitory environment. *Elife,* 10.

874 HE, J., SHENG, T., STELTER, A. A., LI, C., ZHANG, X., SINHA, M., LUXON, B. A. &
875 XIE, J. 2006. Suppressing Wnt signaling by the hedgehog pathway through
876 sFRP-1. *J Biol Chem,* 281**,** 35598-602.
877 HIRSCHBERGER, C., SLEIGHT, V. A., CRISWELL, K. E., CLARK, S. J. & GILLIS,
878 J. A. 2021. Conserved and unique transcriptional features of pharyngeal
879 arches in the skate (Leucoraja erinacea) and evolution of the jaw. *Mol Biol*
880 *Evol,* 38**,** 4187-4204.
881 JEZEWSKI, P. A., FANG, P. K., PAYNE-FERREIRA, T. L. & YELICK, P. C. 2008.
882 Zebrafish Wnt9b synteny and expression during first and second arch, heart,
883 and pectoral fin bud morphogenesis. *Zebrafish,* 5**,** 169-77.
884 JIANG, X., ISEKI, S., MAXSON, R. E., SUCOV, H. M. & MORRISS-KAY, G. M.
885 2002. Tissue origins and interactions in the mammalian skull vault. *Dev Biol,*
886 241**,** 106-16.
887 JURILOFF, D. M., HARRIS, M. J., MCMAHON, A. P., CARROLL, T. J. & LIDRAL, A.
888 C. 2006. Wnt9b is the mutated gene involved in multifactorial nonsyndromic
889 cleft lip with or without cleft palate in A/WySn mice, as confirmed by a genetic
890 complementation test. *Birth Defects Res A Clin Mol Teratol,* 76**,** 574-9.
891 KAGUE, E., GALLAGHER, M., BURKE, S., PARSONS, M., FRANZ-ODENDAAL, T.
892 & FISHER, S. 2012. Skeletogenic fate of zebrafish cranial and trunk neural
893 crest. *PloS One,* 7**,** e47394.
894 KENGAKU, M., CAPDEVILA, J., RODRIGUEZ-ESTEBAN, C., DE LA PENA, J.,
895 JOHNSON, R. L., IZPISUA BELMONTE, J. C. & TABIN, C. J. 1998. Distinct
896 WNT pathways regulating AER formation and dorsoventral polarity in the
897 chick limb bud. *Science,* 280**,** 1274-7.
898 KULAK, O., CHEN, H., HOLOHAN, B., WU, X., HE, H., BOREK, D., OTWINOWSKI,
899 Z., YAMAGUCHI, K., GAROFALO, L. A., MA, Z., WRIGHT, W., CHEN, C.,
900 SHAY, J. W., ZHANG, X. & LUM, L. 2015. Disruption of Wnt/beta-Catenin
901 Signaling and Telomeric Shortening Are Inextricable Consequences of
902 Tankyrase Inhibition in Human Cells. *Mol Cell Biol,* 35**,** 2425-35.
903 LANGMEAD, B., TRAPNELL, C., POP, M. & SALZBERG, S. L. 2009. Ultrafast and
904 memory-efficient alignment of short DNA sequences to the human genome.
905 *Genome Biol,* 10**,** R25.

906 LING, I. T., ROCHARD, L. & LIAO, E. C. 2017. Distinct requirements of wls, wnt9a,
907 wnt5b and gpc4 in regulating chondrocyte maturation and timing of
908 endochondral ossification. *Dev Biol*, 421, 219-232.
909 LU, J., MA, Z., HSIEH, J. C., FAN, C. W., CHEN, B., LONGGOOD, J. C., WILLIAMS,
910 N. S., AMATRUDA, J. F., LUM, L. & CHEN, C. 2009. Structure-activity
911 relationship studies of small-molecule inhibitors of Wnt response. *Bioorg Med*
912 *Chem Lett,* 19**,** 3825-7.
913 LUSTIG, B., JERCHOW, B., SACHS, M., WEILER, S., PIETSCH, T., KARSTEN, U.,
914 VAN DE WETERING, M., CLEVERS, H., SCHLAG, P. M., BIRCHMEIER, W.
915 & BEHRENS, J. 2002. Negative feedback loop of Wnt signaling through
916 upregulation of conductin/axin2 in colorectal and liver tumors. *Mol Cell Biol,*
917 22**,** 1184-93.
918 MAEDA, O., KONDO, M., FUJITA, T., USAMI, N., FUKUI, T., SHIMOKATA, K.,
919 ANDO, T., GOTO, H. & SEKIDO, Y. 2006. Enhancement of GLI1-
920 transcriptional activity by beta-catenin in human cancer cells. *Oncol Rep,* 16**,**
921 91-6.
922 MAO, B., WU, W., DAVIDSON, G., MARHOLD, J., LI, M., MECHLER, B. M.,
923 DELIUS, H., HOPPE, D., STANNEK, P., WALTER, C., GLINKA, A. &
924 NIEHRS, C. 2002. Kremen proteins are Dickkopf receptors that regulate
925 Wnt/beta-catenin signalling. *Nature,* 417**,** 664-7.
926 MARCAIS, G. & KINGSFORD, C. 2011. A fast, lock-free approach for efficient
927 parallel counting of occurrences of k-mers. *Bioinformatics,* 27**,** 764-70.
928 MAXWELL, E. E., FROBISCH, N. B. & HEPPLESTON, A. C. 2008. Variability and
929 conservation in late chondrichthyan development: ontogeny of the winter
930 skate (Leucoraja ocellata). *Anat Rec (Hoboken),* 291**,** 1079-87.
931 NAKAMURA, T., KLOMP, J., PIERETTI, J., SCHNEIDER, I., GEHRKE, A. R. &
932 SHUBIN, N. H. 2015. Molecular mechanisms underlying the exceptional
933 adaptations of batoid fins. *Proc Natl Acad Sci U S A,* 112**,** 15940-5.
934 NIEMANN, S., ZHAO, C., PASCU, F., STAHL, U., AULEPP, U., NISWANDER, L.,
935 WEBER, J. L. & MULLER, U. 2004. Homozygous WNT3 mutation causes
936 tetra-amelia in a large consanguineous family. *Am J Hum Genet,* 74**,** 558-63.
937 NISHIMURA, O., HARA, Y. & KURAKU, S. 2017. gVolante for standardizing
938 completeness assessment of genome and transcriptome assemblies.
939 *Bioinformatics,* 33**,** 3635-3637.

940 O'NEILL, P., MCCOLE, R. B. & BAKER, C. V. 2007. A molecular analysis of
941 neurogenic placode and cranial sensory ganglion development in the shark,
942 Scyliorhinus canicula. *Dev Biol,* 304**,** 156-81.
943 PARR, B. A., SHEA, M. J., VASSILEVA, G. & MCMAHON, A. P. 1993. Mouse Wnt
944 genes exhibit discrete domains of expression in the early embryonic CNS and
945 limb buds. *Development,* 119**,** 247-61.
946 PATRO, R., DUGGAL, G., LOVE, M. I., IRIZARRY, R. A. & KINGSFORD, C. 2017.
947 Salmon provides fast and bias-aware quantification of transcript expression.
948 *Nat Methods,* 14**,** 417-419.
949 PEARSE, R. V., 2ND, VOGAN, K. J. & TABIN, C. J. 2001. Ptc1 and Ptc2 transcripts
950 provide distinct readouts of Hedgehog signaling activity during chick
951 embryogenesis. *Dev Biol,* 239**,** 15-29.
952 PICELLI, S., FARIDANI, O. R., BJORKLUND, A. K., WINBERG, G., SAGASSER, S.
953 & SANDBERG, R. 2014. Full-length RNA-seq from single cells using Smart-
954 seq2. *Nat Protoc,* 9**,** 171-81.
955 RASPOPOVIC, J., MARCON, L., RUSSO, L. & SHARPE. J. 2014. Modeling digits.
956 Digit patterning is controlled by a Bmp-Sox9-Wnt Turing network modulated
957 by morphogen gradients. *Science*, 345, 566-570.
958 REES, J. M. & Gillis, J. A. 2022. Distinct proliferative and middle ear skeletal-
959 patterning functions for SHH-expressing epithelia in the chick hyoid arch. *Dev*
960 *Biol*, 489, 98-108.
961 REID, B. S., YANG, H., MELVIN, V. S., TAKETO, M. M. & WILLIAMS, T. 2011.
962 Ectodermal Wnt/beta-catenin signaling shapes the mouse face. *Dev Biol,* 349**,**
963 261-9.
964 RICHARDSON, J., SHONO, T., OKABE, M. & GRAHAM, A. 2012. The presence of
965 an embryonic opercular flap in amniotes. *Proc Biol Sci,* 279**,** 224-9.
966 ROBINSON, M. D., MCCARTHY, D. J. & SMYTH, G. K. 2010. edgeR: a
967 Bioconductor package for differential expression analysis of digital gene
968 expression data. *Bioinformatics,* 26**,** 139-40.
969 ROCHARD, L., MONICA, S. D., LING, I. T. C., KONG, Y., ROBERSON, S.,
970 HARLAND, R., HALPERN, M. & LIAO, E. C. 2016. Roles for Wnt pathway
971 genes wls, wnt9a, wnt5b, frzb and gpc4 in regulating convergent-extension
972 during zebrafish palate morphogenesis. *Development*, 143, 2541-2547.

973 RUDNICKI, J. A. & BROWN, A. M. 1997. Inhibition of chondrogenesis by Wnt gene
974 expression in vivo and in vitro. *Dev Biol,* 185**,** 104-18.
975 SHIMOMURA, Y., AGALLIU, D., VONICA, A., LURIA, V., WAJID, M., BAUMER, A.,
976 BELLI, S., PETUKHOVA, L., SCHINZEL, A., BRIVANLOU, A. H., BARRES,
977 B. A. & CHRISTIANO, A. M. 2010. APCDD1 is a novel Wnt inhibitor mutated
978 in hereditary hypotrichosis simplex. *Nature,* 464**,** 1043-7.
979 SLEIGHT, V. A. & GILLIS, J. A. 2020. Embryonic origin and serial homology of gill
980 arches and paired fins in the skate, Leucoraja erinacea. *Elife,* 9**,**
981 2020.07.02.183665.
982 SUMMERHURST, K., STARK, M., SHARPE, J., DAVIDSON, D. & MURPHY, P.
983 2008. 3D representation of Wnt and Frizzled gene expression patterns in the
984 mouse embryo at embryonic day 11.5 (Ts19). *Gene Expr Patterns,* 8**,** 331-48.
985 SUN, X., ZHANG, R., CHEN, H., DU, X., CHEN, S., HUANG, J., LIU, M., XU, M.,
986 LUO, F., JIN, M., SU, N., QI, H., YANG, J., TAN, Q., ZHANG, D., NI, Z.,
987 LIANG, S., ZHANG, B., CHEN, D., ZHANG, X., LUO, L., CHEN, L. & XIE, Y.
988 2020. Fgfr3 mutation disrupts chondrogenesis and bone ossification in
989 zebrafish model mimicking CATSHL syndrome partially via enhanced
990 Wnt/beta-catenin signaling. *Theranostics,* 10**,** 7111-7130.
991 TAKENAKA, K., KISE, Y. & MIKI, H. 2007. GSK3beta positively regulates Hedgehog
992 signaling through Sufu in mammalian cells. *Biochem Biophys Res Commun,*
993 353**,** 501-8.
994 TEN BERGE, D., BRUGMANN, S. A., HELMS, J. A. & NUSSE, R. 2008. Wnt and
995 FGF signals interact to coordinate growth with cell fate specification during
996 limb development. *Development,* 135**,** 3247-57.
997 THIERY, A.P., STANDING, A.S., COOPER, R.L. & FRASER, G.J. 2022. An
998 epithelial signalling centre in sharks supports homology of tooht
999 morphogenesis in vertebrates. *eLife*, 11, e73173.
1000 VEITCH, E., BEGBIE, J., SCHILLING, T. F., SMITH, M. M. & GRAHAM, A. 1999.
1001 Pharyngeal arch patterning in the absence of neural crest. *Curr Biol,* 9**,** 1481-
1002 4.
1003 WALL, N. A. & HOGAN, B. L. 1995. Expression of bone morphogenetic protein-4
1004 (BMP-4), bone morphogenetic protein-7 (BMP-7), fibroblast growth factor-8
1005 (FGF-8) and sonic hedgehog (SHH) during branchial arch development in the
1006 chick. *Mech Dev,* 53**,** 383-92.

1007 WITTEN, P. E. & HALL, B. K. 2003. Seasonal changes in the lower jaw skeleton in
1008 male Atlantic salmon (Salmo salar L.): remodelling and regression of the kype
1009 after spawning. *J Anat,* 203**,** 435-50.
1010 ZHANG, X., CHEONG, S. M., AMADO, N. G., REIS, A. H., MACDONALD, B. T.,
1011 ZEBISCH, M., JONES, E. Y., ABREU, J. G. & HE, X. 2015. Notum is required
1012 for neural and head induction via Wnt deacylation, oxidation, and inactivation.
1013 *Dev Cell,* 32**,** 719-30.